Available online at www.sciencedirect.com
SCIENCE DIRECT®
Mechanics of Materials 37 (2005) 753–767
MECHANICS OF MATERIALS
www.elsevier.com/locate/mechmat

Grain refinement versus voids accumulation during severe plastic deformations of polycrystals: mathematical simulation

Y. Beygelzimer *

Donetsk Physics and Technology Institute named after A.Galkin of the Ukrainian Academy of Sciences, 72 R. Luxembourg St., Donetsk, 83114, Ukraine

Received 6 April 2004; received in revised form 8 July 2004

Abstract

We view the emergence of disorientation boundaries in crystals and the formation of micropores as complementary mechanisms of relaxation of internal strain during severe plastic deformations of polycrystals. Using an assumption of self-similarity of the grain refinement process, we obtain kinetic equations for two scalar parameters characterizing the structure of the material: the total area of fragment boundaries and the total volume of micropores per unit volume of material. We show that the model captures the main regularities of large plastic deformations of metals with high stacking-fault energy. The analysis of the model yields a number of recommendations for increasing the effectiveness of severe plastic deformation processes.

Keywords: Severe plastic deformation; Grain refinement; High-angular boundary; Void; Ductility; Self-similarity

1. Introduction

Recently there has been a lot of interest in ultrafine grained materials obtained using severe plastic deformations (SPD). Investigations show that such materials possess a unique combination of high strength and ductility (Valiev et al., 2000).

SPD methods are based on metal forming processes that guarantee both strain accumulation and intense grains refinement. Such processes include equal channel angular extrusion (Segal, 2002; Valiev et al., 2000), twist extrusion (Beygelzimer et al., 2002), and multiple forging (Valiev et al., 2000). When developing SPD methods, one needs to be able to predict grains refinement and ductile failure of the deformed materials during large plastic deformation.

* Fax: +38 62 3377608.

0167-6636/$ - see front matter © 2004 Published by Elsevier Ltd.
doi:10.1016/j.mechmat.2004.07.006

There are a number of models allowing one to track changes in structural characteristics of metals during metal forming processes (e.g., Tvergaard, 1992; Raabe, 1998; Kolmogorov, 1997; Beygelzimer et al., 1994). None of them, however, takes into account the relation between grain refinement and ductile failure.

In this paper, we develop such a model for describing the processes of grain refinement and ductile failure of metals with high stacking-fault energy. For this, we introduce two scalar parameters characterizing the structure of the material: the total area of fragment boundaries and the total volume of micropores per unit volume of material. Under certain assumptions, we obtain kinetic equations for the above parameters. The analysis of the model shows that it captures the main regularities of large plastic deformations of metals with high stacking-fault energy. This gives us that it could be used to analyze the metal forming processes of such metals; in particular, SPD processes.

2. Physical prerequisites of the model

The model is based on the following results of physical investigations.

According to the Le-Chatelie principle, the external load applied to material that results in elastic deformations of the crystal lattice, triggers the processes that tend to weaken the effect of this load, i.e. to decrease the deformations that it causes. If the loading process is viewed from this stand point, it follows that metals do not harden under plastic deformation; on the contrary, they try to reduce the external load by decreasing elastic deformations.

Materials are not homogeneous, and the above processes represent the transfer of atoms from the sites of the maximum compression to the sites where the compression stress is lower.

Polycrystalline materials have several elementary mechanisms of substance transfer (for example, dislocation slip, transverse dislocation motion, diffusion, twinning), each having its own activation energy and providing its own strain rate for given parameters of external influence (stress, strain rate, temperature).

Under given conditions, the primary mechanisms controlling the deformation are those that ensure the highest strain rate, i.e. reduce the external load more effectively than others (Frost and Ashby, 1982).

Since the material structure is heterogeneous, the plastic deformation of the material as a whole can only be realized through a joint deformation of individual structural elements, i.e. homogeneous crystallite regions. According to R. Mises, such structural element can be deformed arbitrarily if it has five independent slip systems. Due to mutual hardening, there are at most two or three such systems present. Thus during deformation, the shear becomes locked inside the structural elements, and as a result the inner microstresses increase and cause strain hardening at comparatively low equivalent strain.

Since internal stresses are highly non-uniform, they result in bending and twisting of the crystal lattice; these effects become more pronounced as the strain increases. The stress relaxation is possible either via relative rotation of the lattice elements leading to partial disclination (Rybin, 1986), or the formation of micropores with dimension of cross-section around 100 nm (Cheremskoj et al., 1990). The first way results in grain refinement of crystallites, and thus in material hardening; the second—in the increase of structural damage and in the decrease of ductility.

Micropores practically do not change in size during the deformation of the material, and the fracture process is basically a gradual accumulation of micropores. When the concentration of micropores reaches a certain limit (nearly 0.01 of the material volume), the macroscopic crack start to form (Cheremskoj et al., 1990). This limit is taken as a criterion for macroscopic fracture during plastic deformation under pressure (Beygelzimer et al., 1994)).

The probabilities with which the above mentioned ways of stress relaxation are realized, are determined by material properties, pressure, temperature, and strain rate. With the increase of the value of pressure, the probability of micropore formation typically decreases, and stress relaxation is achieved through formation of disorientation boundaries.

There are two main scenarios of material structure evolution that realize in metals with low and high stacking-fault energy (SFE) respectively (Rybin, 1986). The model developed below focuses on the second class of materials, thus we mostly consider the regularities of grain refinement in this case.

Metals with high SFE allow for a rather free transverse motion of dislocations, which initially provides substance migration from sites of compression to sites of tension. This results in a temporary relaxation of elastic bends and the formation of low-disoriented cells. With further loading, the stress continues to grow and some relaxation of the growing bendings of the lattice becomes necessary. This leads to the formation of disclinations, mobile concentrators of stress; such concentrators start to form in places of high curvature or twisting of the lattice, i.e., in regions of where stress is concentrated (most often at grain boundaries). The disclinations then move inside the crystal, transforming strong elastic bends of the crystal lattice into high-angle boundaries of discrete disorientation. A disclination is a concentrator of momentary stress, while the substance is transferred by dislocations.

Disclinations are moving along "marked paths", i.e., cell boundaries. This movement causes the formation of fine, roughly equiaxed, highly disoriented fragments.

3. Basic assumptions and notions

First, let us consider those regions of crystals in which dislocation charges accumulate to such extent that it leads to the emergence of either a micropore or a new branch of a high angular boundary. We call such regions accumulation zones (AZ for short). AZs emerge due to inhomogeneities of shear along the sliding planes. This happens because the shear causes the region of the crystal in which it occurs to turn (Nemat-Nasser and Hori, 1999). Shear deformation is characterized by high gradients on the boundary between crystallines and in those places where crystallines are highly inhomogeneous. This causes the differences in the angles of adjacent regions, which in turn leads to accumulation of bends and twists of the crystalline lattice at the point where the regions join. The regions where the lattice becomes locally distorted are precisely the AZs.

At a high enough magnitude of bends and twists of the crystal lattice, AZs start to relax. We assume that this relaxation occurs either through formation of high-angle boundary nuclei (BN for short), or emergence of micropores. The first results in grain refinement, the second in material failure. The scheme in Fig. 1 explains the origin of AZ emergence, structure, and possible relaxation types.

The size of an AZ can be estimated by the diameter of a micropore which emerges during stress relaxation in that zone. According to (Cheremskoj et al., 1990), this size is of the order of 100 nm.

According to (Rybin, 1986; Cheremskoj et al., 1990), we assume that rearrangements of the crystal structure related to the emergence of micropores and "nuclei" of high-angular boundaries, take much less than the characteristic time of deformation. On the other hand, we assume that other relaxation processes do not have time to occur during the deformation. This assumption is true for cold plastic deformation, and it enables one to treat the equivalent strain as a monotonously growing parameter determining the sequence of loading stages. Fixing this parameter, i.e., stopping the loading, "freezes" the material

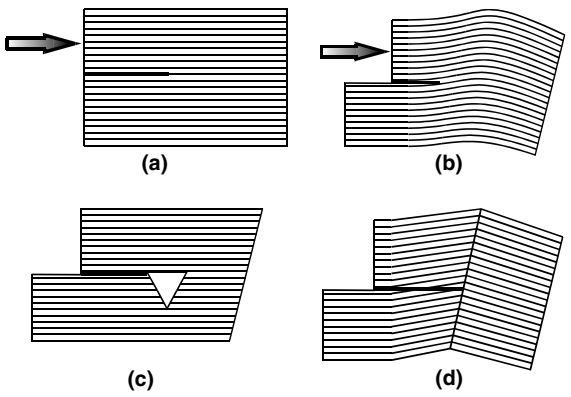

Fig. 1. A scheme explaining creation of an accumulative zone under a non-uniform shear in crystal (a, b), its relaxation by micropore (c), and formation of a high angular boundary nucleus (d).

structure and fixes all the values that characterize this structure.

As a physical model of BN we use a partial disclination, which represents a mobile concentrator of stress transforming the bends of the crystal lattice into a high-angle boundary.

We use the total length of boundaries per unit of cross-section area of the representative volume element (denoted by S) to measure the extent to which the network of high-angle boundaries is developed.

A quantitative measure of the degree of failure of the representative volume element is the total volume of pores Θ per unit volume of the material.

According to (Rybin, 1986), we distinguish between highly disoriented regions in the structure of crystallite (with disorientation angle larger than 10–20°), fragments and regions with low disorientation angle (of the order of several minutes), and finally cells.

Each fragment is a group of cells surrounded by high-angle boundaries. The latter form a network with average unit size of $L \approx 1/(S_0 + S)$, where S_0 is the length of grain boundaries per unit of cross-section area. Cell boundaries form a small network with grain size d_c, and according to (Rybin, 1986), high angular boundaries propagate along the network. This means that d_c is the minimum size of a high angular boundary region or the smallest fragment size. This size is determined by material composition, temperature, strain rate, but it is independent of the initial material structure and the type of loading.

In this paper, we estimate the cell size using experimental data from the paper (Rybin, 1986), where it is shown that for metals $d_c \approx 100\,\text{nm}$.

We assume that when $d_c \ll L \ll L_0$ (or equivalently, $S_0 \ll S \ll S_c$, where $L_0 = \frac{1}{S_0}$ is the average grain size, and $S_c = \frac{1}{d_c}$ is the length of the cellular network per unit of cross-section area) and if there is practically no change in loading conditions for the representative volume element of the material (during quasi-monotonic loading), the mesh of high angular boundaries develops in a self-similar fashion. This means that the meshes of high angular boundaries during consecutive steps of loading are geometrically similar (in the statistical sense).

This assumption is based on the analysis of microstructures given in papers (Rybin, 1986; Langford, 1970; Langford and Cohen, 1969, 1975). The assumption is justified by the invariance of grain refinement mechanisms for $d_c \ll L \ll L_0$ and the fact that loading conditions are fixed.

There exists an explicit analogy between the grain refinement process and some other phenomena (e.g., onset turbulence, quasi-brittle fracture), where the assumption of self-similarity made it possible to significantly simplify the problem and led to results that agree with observed experimental results (Barenblatt, 1979; de Gennes, 1979).

Self-similarity in the development of a geometrical set leads to the formation of fractal structures (Mandelbrot, 1983). So it is not unexpected to that self-similarity of the grain refinement process leads to fractal structure of the set of high angular boundaries. We will use this observation for deriving the Hall–Petch relationship within the framework of our model.

Also we note that self-similarity of the grain refinement process results in a fractal structure of the polycrystal yield surface (Beygelzimer and Spuskanyuk, 1999; Beygelzimer et al., 2001).

According to Kolmogorov (1941), if iterative partitioning of an object occurs in a self-similarity way, i.e. the law that defines how an object is divided into smaller ones does not depend on the size of the object, then fragment sizes are distributed according to a lognormal distribution. Such a conclusion is in agreement with several SPD experiments (Valiev et al., 2000; Langford and Cohen, 1975), which can be viewed as an evidence in favor of the assumption of self-similarity of the fragmentation process.

The density of the lognormal distribution is given by (Kolmogorov, 1941):

$$f(\xi) = \begin{cases} \frac{1}{\xi\kappa\sqrt{2\pi}} \exp\left(-\frac{\left(\ln\left(\frac{\xi}{\overline{\xi}}\right) + 0.5\kappa^2 \right)^2}{2\kappa^2} \right) 0, & \text{if } \xi \le 0, \\ 0, & \text{if } \xi > 0, \end{cases} \tag{1}$$

where $\overline{\xi}$ is the mean of the random variable ξ, which in our case equals S^{-1}; and κ is the para-

meter characterizing the width of the interval containing most of the probability mass of ξ.

4. Basic relationships of the model

Let us consider a flat section of the representative volume of a polycrystal. According to the model, the objects we defined above (accumulative zones, "nuclei" of high angular boundaries, and micropores) correspond to points in this section, provided that the size of the representative volume element is much larger than that of these objects. We denote the number of AZs by N, and high-angle boundary nucleation per unit of polycrystal section by N_b. We will derive kinetic equations for given N, N_b , S and Θ.

Assume that the increment dN_1 of the number of accumulative zones that is due to their formation at the obstacles present in the initial structure of the material (before the plastic deformation starts) is proportional to the increment of the degree of the representative-volume strain. In symbols,

$$\mathrm{d}N_1 = \frac{C_1}{\Delta^2}\,\mathrm{d}\gamma, \tag{2}$$

where C_1 is the parameter dependent on the composition and structure of the material, as well as on the stress state of the representative volume element, the temperature and the strain rate of deformation; γ is the intensity of the representative-volume shear deformation; Δ (to be defined later) is some characteristic size of the structure introduced for dimensionality reasons.

During a large plastic deformation, the structure of the material changes, which is immediately evidenced by the increase in the area of high angular boundaries. Their role in the AZ originations is dual. New boundaries represent additional obstacles in the motion of dislocations; this results in nucleation of new AZs. On the other hand, since the boundaries of the deformation origin are typically non-equilibrium, the increase of their area increases the probability of stress relaxation through the rotation of fragments with slippage along the boundaries. This decreases the rate of AZ formation.

Let us express the described effects mathematically. For $d_\mathrm{c} \ll L \ll L_0$, fragment boundaries can be represented as lines having obstacles in going through boundary shear. From the self-similarity in the development of the network of high angular boundaries, it follows that the average number of obstacles C_2 per one link of the network, remains unchanged. Since a plastic deformation typically covers a comparatively small volume of the material, and is a very small fraction of network links nucleates a new high angular boundary at any given moment, we have $C_2 < 1$. The analysis of structures shows that $C_2 \approx 0.1$.

It follows that for $d_\mathrm{c} \ll L \ll L_0$, an increment in the number of AZs due to the increase of the length of high angular boundaries by the value of $\mathrm{d}S$, is given by

$$\mathrm{d}N_2 = \frac{C_2}{L}\,\mathrm{d}S = C_2(S_0 + S)\,\mathrm{d}S. \tag{3}$$

Adding (2) and (3), we have

$$\mathrm{d}N = \left(\frac{C_1}{\Delta^2} + C_2(S_0 + S)\frac{\mathrm{d}S}{\mathrm{d}\gamma}\right)\mathrm{d}\gamma. \tag{4}$$

When magnitude L becomes comparable to d_c, the sections of an easy passage of the boundary shear start interacting with one another. This results in the stress relaxation in regions of inhomogeneous shear and in the decrease in the rate of AZ formation. The later becomes zero when $L \approx d_\mathrm{c}$, since fragments of this size can no longer be divided.

We will take this into account in the model. To do this, we introduce a cofactor $F(S)$ into the right hand part of relation (4). For $S_0 \ll S \ll S_\mathrm{c} \approx d_\mathrm{c}^{-1}$ ($d_\mathrm{c} \ll L \ll L_0$), the value of $F(S)$ is practically equal to 1, and it vanishes to 0 for $S \to S_\mathrm{c}$ ($L \to d_\mathrm{c}$). The physical meaning of $F(S)$ is the fraction of fragments undergoing division under the plastic deformation.

After incorporating this change into the model, we get a new version of Eq. (4):

$$\mathrm{d}N = \left(\frac{C_1}{\Delta^2} + C_2(S_0 + S)\frac{\mathrm{d}S}{\mathrm{d}\gamma}\right)F(S)\,\mathrm{d}\gamma. \tag{5}$$

We can now derive an expression for $F(S)$.

First, notice that for sufficiently small sizes, the curve for the lognormal distribution has a section

with an almost zero ordinate. This happens because as the value $\frac{d}{\overline{d}}$ decreases in the interval $0 < \frac{d}{\overline{d}} < 1$, its logarithm swiftly grows in the absolute value, which leads to large negative values in the exponent. The smallest boundary point d^*, where the distribution function becomes significantly different from zero, is determined from the condition that the exponent at this point becomes of order—10. Thus we have:

$$d^* \approx \overline{d} \exp\left(-\kappa\sqrt{20}\right). \tag{6}$$

In the course of the fragmentation process, the distribution of fragment sizes varies. As long as the point with coordinate d_c is in the "zero ordinate" section, the fraction of indivisible fragments can be neglected. At the point defined by the condition $d^* \approx d_c$, this fraction is no longer negligible. The number of such segments keeps growing, and the distribution of fragment sizes is no longer lognormal.

We take the indivisible fragments as a separate group, while the rest will be assumed to be distributed according to the lognormal law. In this case, $F(S)$ is the fraction of fragments in the second group, and $(1 - F(S))$—in the first group.

As the fragments of dimensions d_c immediately get transferred to the first group, the boundary d^* of the curve corresponding to the distribution in the second group should be at point d_c at all times. Then it follows from relationship (6) that the average fragment size $\overline{d}_2$ in the second group remains constant, and is given by the formula:

$$\overline{d}_2 \approx d_c \exp\left(\kappa\sqrt{20}\right). \tag{7}$$

The average of all fragment sizes, S^{-1}, is a weighted mean of the respective averages in the first and the second group, i.e.,

$$S^{-1} = F(S)\overline{d}_2 + (1 - F(S))d_c. \tag{8}$$

Once the left boundary of the lognormal distribution reaches the value of d_c, the value of $F(S)$ follows from Eqs. (7) and (8):

$$F(S) = \frac{\frac{S_c}{S} - 1}{\exp\left(\kappa\sqrt{20}\right) - 1}. \tag{9}$$

When the left boundary is still greater than d_c, we have $F(S) = 1$.

The value of S corresponding to the transition can be obtained from relationship (7), since at this moment $S^{-1} = \overline{d}_2$.

Thus the value of $F(S)$ is given by the following expression:

$$F(S) = \begin{cases} 1 & \text{if } \frac{S}{S_c} < \exp\left(-\kappa\sqrt{20}\right), \\ \dfrac{\frac{S_c}{S} - 1}{\exp\left(\kappa\sqrt{20}\right) - 1} & \text{if } \exp\left(-\kappa\sqrt{20}\right) \leqslant \frac{S}{S_c} < 1, \\ 0 & \text{if } \frac{S}{S_c} \geqslant 1, \end{cases} \tag{10}$$

Fig. 2 shows a plot of this function for $\kappa = 0.2$.

We now derive an expression for dN. According to the kinetic theory, the average time before the formation of a micropore in the accumulative zone is given by the relationship

$$t_p = v^{-1} \exp\left(\frac{U_p - \omega_p(\sigma - p)}{kT}\right), \tag{11}$$

where U_p is the activation energy of pore formation in the absence of mechanical stress; σ is tensile stress in the accumulative zone due to the deformation of the crystal lattice; p is the hydrostatic pressure from the external stress applied to the representative volume element; ω_p is a parameter of the material (called the activation volume); k is the Boltzmann's constant, v is the oscillation frequency for the crystalline lattice.

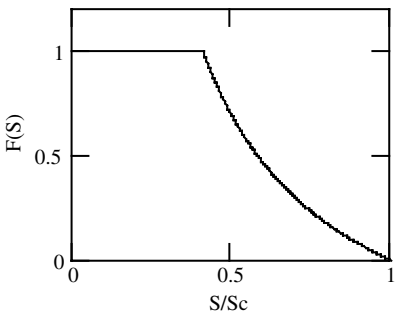

Fig. 2. Fraction of fragments subjected to division as a function of $\frac{S}{S_c}$.

Similarly, the average time before the formation of a high angular boundary "nucleus" in the accumulative zone is

$$t_b = v^{-1} \exp\left(\frac{U_b - \omega_b \tau}{kT}\right), \tag{12}$$

where U_b is the activation energy of nucleus formation in the absence of mechanical stresses; τ is the intensity of tangential stress due to the deformation of the crystalline lattice in the accumulative zone; ω_b is a parameter of the material.

Relationships (11) and (12) show that under a low-temperature deformation (i.e., when $kT \to 0$), the processes of pore formation and high angular boundary "nucleation" exhibit a threshold behavior, i.e. appear suddenly at threshold values σ_c and τ_c defined by the relationships:

$$\sigma_c = \frac{U_p}{\omega_p} + p, \tag{13}$$

$$\tau_c = \frac{U_b}{\omega_b}. \tag{14}$$

Parameters U_p, U_b, ω_p, and ω_b depend on the material structure in the accumulative zone; so in different AZs, the values of σ_c and τ_c can be different.

Thus in the AZs, the internal stress increases in the course of the plastic deformation. At the moment when the stress reaches the value of σ_c (or τ_c), the AZs instantaneously relax leading to the formation of micropores (or nuclei of high angular boundaries).

Let $\gamma_p(p)$ be the mean strain of the quasi-monotonous deformation necessary for the tensile stress to reach its critical value. The value of γ_p is a function of p, because according to (13), the value of σ_c, and thus of γ_p, increases with the hydrostatic pressure in the representative volume element of the material.

The probability P of pore formation in an AZ during deformation accumulation is given by

$$P = 1 - \exp\left(-\frac{\gamma}{\gamma_p(p)}\right). \tag{15}$$

For $\gamma \ll 1$, it follows from that

$$P = \frac{\gamma}{\gamma_p(p)}. \tag{16}$$

When the deformation is incremented by some small value $d\gamma$, the number of AZs decreases (due to pore formation) by

$$dN_p = -N\,dP = -N\frac{d\gamma}{\gamma_p(p)} \tag{17}$$

Similarly, a decrease in the number of AZs due to the formation of nuclei of high angular boundaries is defined by the relationship:

$$dN_b = -N\,dP = -N\frac{d\gamma}{\gamma_b}, \tag{18}$$

where γ_b is the average degree of the quasi-monotone deformation necessary for the tangential stress in an AZ to reach its critical value.

Taking into account that $dN = dN_p + dN_b$, we have that

$$dN = -(C_3(p) + C_4)N\,d\gamma, \tag{19}$$

where

$$C_3(p) = \frac{1}{\gamma_p(p)}, \quad C_4 = \frac{1}{\gamma_b}. \tag{20}$$

Adding Eqs. (5) and (19), we have

$$dN = \left(\frac{C_1}{\Delta^2} + C_2(S_0 + S)\frac{dS}{d\gamma}\right)F(S)\,d\gamma - (C_3(p) + C_4)N\,d\gamma. \tag{21}$$

We take d_c as the characteristic size of the structure Δ, and introduce dimensionless functions (denoted by a bar above the notation):

$$\overline{N} = Nd_c^2 = \frac{N}{S_c^2}, \quad \overline{N}_b = N_b d_c^2 = \frac{N_b}{S_c^2},$$
$$\overline{S} = Sd_c = \frac{S}{S_c}, \quad \overline{S}_0 = S_0 d_c = \frac{S_0}{S_c}. \tag{22}$$

In dimensionless variables, Eq. (21) takes the following form:

$$d\overline{N} = \left(C_1 + C_2(\overline{S}_0 + \overline{S})\frac{d\overline{S}}{d\gamma}\right)F(\overline{S})\,d\gamma - (C_3(p) + C_4)\overline{N}\,d\gamma. \tag{23}$$

We derive a differential equation for the number $\overline{N}_b$ of "nuclei" of high angular boundaries. The nucleation is described by the relationship:

$$d\overline{N}_b = C_4\overline{N}\,d\gamma. \tag{24}$$

As mentioned above, BNs are mobile stress concentrators (a partial disclination), which—when moving through the material under deformation—leave a high angular boundary trace. If a concentrator comes across another such boundary, it dies. Therefore, the mean length of their free run is given by $\overline{L} \approx \frac{1}{\overline{S}+\overline{S}_0}$, the length of a single link of the network formed by high angular boundaries.

It is natural to assume that when the concentrators are shifted by $\mathrm{d}\overline{l}$, the quantity of dead BNs is given by $\mathrm{d}\overline{N}_\mathrm{b} = -\overline{N}_\mathrm{b}\frac{\mathrm{d}\overline{l}}{\overline{L}}$. The value of $\mathrm{d}\overline{l}$ is proportional to $\mathrm{d}\gamma$. It follows from the assumption of self-similarity of the ensemble of boundaries that

$$\mathrm{d}\overline{l} = C_5\overline{L}\,\mathrm{d}\gamma. \tag{25}$$

Substituting this relationship into relationship (24), we get $\mathrm{d}\overline{N}_\mathrm{b} = -C_5\overline{N}_\mathrm{b}\,\mathrm{d}\gamma$. Adding relationship (24), yields

$$\mathrm{d}\overline{N}_\mathrm{b} = C_4\overline{N}\,\mathrm{d}\gamma - C_5\overline{N}_\mathrm{b}\,\mathrm{d}\gamma. \tag{26}$$

Relationship (25) gives a differential equation for $\overline{S}$:

$$\mathrm{d}\overline{S} = \frac{C_5\overline{N}_\mathrm{b}\,\mathrm{d}\gamma}{\overline{S}+\overline{S}_0}. \tag{27}$$

Changes in the value of metal porosity Θ during plastic deformation are due to the processes of micropore "nucleation" and "healing". As a result, we have the following differential equation

$$\mathrm{d}\Theta = vN_vC_3\,\mathrm{d}\gamma - C_6\Theta\,\mathrm{d}\gamma, \tag{28}$$

where N_v is the number of AZs in the unit volume of the material; v is the volume of a micropore; and C_6 is a parameter defined below.

The first term of the right hand side of (28) follows from relationships (17) and (20), and describes micropore nucleation. The second term reflects the processes of micropore healing during metal deformation under pressure, and considers the intensity of the process to be proportional to the porosity value (Beygelzimer et al., 1994). In first approximation, $N_v = N^{\frac{3}{2}}$.

Substituting this relationship into (28) with (22) taken into consideration, we have:

$$\mathrm{d}\Theta = C_3\left(\overline{N}d_\mathrm{c}^2\right)^{\frac{3}{2}}v\,\mathrm{d}\gamma - C_6\Theta\,\mathrm{d}\gamma. \tag{29}$$

We finally combine Eqs. (23), (26), (27), and (29) to get a system of differential equations that describe a joint effect of metal grain refinement and metal failure during plastic deformation under pressure:

$$\begin{cases} \dfrac{d\overline{N}}{\mathrm{d}\gamma} = \left(C_1 + C_2C_5\overline{N}_\mathrm{b}\right)F\left(\overline{S}\right) - (C_3+C_4)\overline{N}, \\ \dfrac{\mathrm{d}\overline{N}_\mathrm{b}}{\mathrm{d}\gamma} = C_4\overline{N} - C_5\overline{N}_\mathrm{b}, \\ \dfrac{\mathrm{d}\overline{S}}{\mathrm{d}\gamma} = \dfrac{C_5\overline{N}_\mathrm{b}}{\overline{S}+\overline{S}_0}, \\ \dfrac{\mathrm{d}\Theta}{\mathrm{d}\gamma} = C_3\overline{N}^{\frac{3}{2}}d_\mathrm{c}^{-3}v - C_6\Theta. \end{cases} \tag{30}$$

In the case of quasi-monotone loading, the initial conditions for solving system (30) should be $\overline{N} = 0$, $\overline{N}_\mathrm{b} = 0$, $\overline{S} = 0$, and $\Theta = 0$, for $\gamma = 0$.

To describe non-monotone loading, the entire process has to be divided into quasi-monotonous stages, and system (30) must be solved for each stage separately.

As initial values of $\overline{N}_\mathrm{b}$, $\overline{S}$, and Θ at any stage (except the first one), one should take finite values of these parameters computed during the previous stage. For any stage, the initial value for $\overline{N}$ is $\overline{N} = 0$, which means that an abrupt change in the direction of material loading leads to a relaxation of AZs.

5. The analysis

Let us analyze the system of equations obtained above. Setting the right-hand sides of (30) to zero and solving the resulting system of algebraic equations, we get a single stationary (i.e., not changing with the growth of deformation) solution:

$$\overline{N} = 0, \quad \overline{N}_\mathrm{b} = 0, \quad \overline{S} = 1, \quad \Theta = 0. \tag{31}$$

It is easy to see that all solutions of system (30) tend, at the limit of large γ, to this stationary solution. Thus the model implies that metals during large quasi-monotone deformations obtain some stationary microstructure with the average fragment size d_c independent of the type of loading.

Deformation of a material with a stationary structure occurs in the absence of failure ($\Theta = 0$). There is no hardening, since the surface of fragments per unit volume of material remains constant. A physical reason of such an effect is a relaxation of lattice bending-twisting due to a possible slippage of fine fragments.

When the average fragment size is much larger than d_c (i.e., $\overline{S} \ll 1$), then $F(\overline{S})$ is practically one. In this case, system (30) reduces to a system of two linear differential equations:

$$\begin{cases} \dfrac{d\overline{N}}{d\gamma} = C_1 + C_2C_5\overline{N}_b - (C_3 + C_4)\overline{N}, \\ \dfrac{d\overline{N}_b}{d\gamma} = C_4\overline{N} - C_5\overline{N}_b, \end{cases} \tag{32}$$

and two remaining differential equations for $\overline{S}$ and Θ.

The two roots of the characteristic equation of system (32) are

$$\lambda_{1,2} = -\frac{C_3 + C_4 + C_5}{2} \pm \frac{\sqrt{(C_3 + C_4 - C_5)^2 + 4C_2C_4C_5}}{2}. \tag{33}$$

It follows from the latter relationship that for $C_2 > 1 + \frac{C_3}{C_4}$, one of the roots is positive. This results in an exponentially increasing solution of system (32).

Recall that C_2 is the number of AZs per unit length of the network of high angular boundaries. As noted above, typically $C_2 \ll 1$. In this case

$$\lambda_1 = -C_5 < 0, \quad \lambda_2 = -(C_3 + C_4) < 0, \tag{34}$$

and as deformation increases, all solutions of system (32) tend to the stationary solution:

$$\overline{N} = \frac{C_1}{C_3 + C_4}, \quad \overline{N}_b = \frac{C_1C_4}{C_5(C_3 + C_4)}. \tag{35}$$

The value of strain, γ^*, after which both $N(\gamma)$ and $N_b(\gamma)$ practically take the above values, is defined by the relationship $\gamma^* \approx \frac{1}{\lambda}$, where $\lambda = \min(|\lambda_1|, |\lambda_2|)$.

Solution (35), according to the third equation of system (32), corresponds to the following relationship for $\overline{S}$ (when $\overline{S} \gg \overline{S}_0$):

$$\overline{S} = \sqrt{\frac{2C_1C_4}{C_3 + C_4}}\sqrt{\gamma}, \tag{36}$$

and the following differential equation for Θ:

$$\frac{d\Theta}{d\gamma} = C_3\left(\frac{C_1}{C_3 + C_4}\right)^{\frac{3}{2}} d_c^{-3}v - C_6\Theta. \tag{37}$$

According to the self-similarity hypothesis, when the value of deformation is γ_2, the geometric pattern of the boundaries ensemble is similar to that at moment γ_1, the only difference being that the scale factor is $f = f\left(\frac{\gamma_2}{\gamma_1}\right)$. This function should satisfy an obvious condition $f\left(\frac{\gamma_3}{\gamma_1}\right) = f\left(\frac{\gamma_2}{\gamma_1}\right)f\left(\frac{\gamma_3}{\gamma_2}\right)$, from which it follows that $f \sim \left(\frac{\gamma_2}{\gamma_1}\right)^n$. Comparing this dependence and Formula (36) shows that, in our case, $n = 0.5$.

Relationship (37) coincides with the differential equation for porosity arising from a continual model of porous body with a structurally non-uniform frame (Beygelzimer et al., 1994):

$$\frac{d\Theta}{d\gamma} = \alpha - 6a\frac{p}{K}\Theta, \tag{38}$$

where α is the so-called accommodation parameter showing that structure elements of the material can partially accommodate each other during plastic deformation; a is a parameter characterizing the morphology of pores; K is shear yield stress.

Comparing Eqs. (37) and (38), we get:

$$C_3\left(\frac{C_1}{C_3 + C_4}\right)^{\frac{3}{2}} d_c^{-3}v = \alpha, \tag{39}$$

$$C_6 = 6a\frac{p}{K}. \tag{40}$$

A continual model of metal failure under plastic deformations has been developed in (Beygelzimer et al., 1994). The model is based on Eq. (38) and a criterion of failure, according to which a macroscoping-scale crack originates at some critical value of porosity Θ_c which depends neither on the material nor on the stress state. This criterion was proposed in (Cheremskoj et al., 1990), where it was shown experimentally that $\Theta_c \approx 0.01$.

The following relationship for metal plasticity γ_p (value of strain before fracture when $\frac{p}{K}$ is constant) was derived in (Beygelzimer et al., 1994):

$$\gamma_p = \frac{1}{3a(p/K)} \ln\left[1 + 3a(p/K)\frac{\Theta_c}{\alpha}\right]. \quad (41)$$

This relationship allows one to determine parameters α and a from the experimental dependency $\gamma_p = \gamma_p\left(\frac{p}{K}\right)$, called the diagrams of plasticity (available in the literature).

Note than the diagrams of plasticity depend considerably on the loading mode. The smallest value of deformation before fracture is typically obtained in simple shear experiments (Kolmogorov, 1997).

Relationship (41) gives a simple expression for parameter α:

$$\alpha = \frac{\Theta_c}{\gamma_{p0}}, \quad (42)$$

where γ_{p0} is the deformation prior to fracture assuming zero value of hydrostatic stress.

We express coefficient C_1 through the value of α using relationship (39):

$$C_1 = (C_3 + C_4)\left(\frac{\alpha d_c^3}{C_3 v}\right)^{\frac{2}{3}}. \quad (43)$$

Substituting this expression into expression (36), we get

$$\overline{S} = \sqrt{2C_4}\left(\frac{\alpha d_c^3}{C_3 v}\right)^{\frac{1}{3}}\sqrt{\gamma}. \quad (44)$$

This relationship shows that the higher the values of α and C_4, and the lower the value of C_3, the higher the intensity of grain refinement.

The value of $C_3(p)$ decreases with the increase of hydrostatic pressure. The pressure does not influence any other parameter in (44). Hence the higher the pressure, the more intense grain refinement.

From relationship (42), it follows that α is higher for those modes of loading for which plasticity is lower. Thus the processes that yield higher failure (among the processes with comparable hydrostatic pressure in the center of deformation) result in a more intensive fragmentation. For obtaining submicro- and nanostructures, such processes should be carried out under high hydrostatic pressure. In this case, the relaxation of internal stresses goes via crystallite grain refinement, not via formation of micropores.

As mentioned above, the smallest value of ductility is typically observed in schemes based on simple shear. Thus simple shear under high pressure is probably the most effective for obtaining submicro-structures. This is in compliance with experimental results given in (Segal, 2002).

We now analyze the set of solutions of system (30) using a typical numerical example. We need to evaluate model parameters. Let us take $\gamma_p \approx 0.2$ (following Rybin, 1986; Langford, 1970) and $\gamma_b \approx 0.4$ (following Cheremskoj et al., 1990). From expression (22), we have $C_3 \approx 5$ and $C_4 \approx 2.5$.

Quantity C_1 is estimated from relationship (43). Let us take $\alpha \approx 0.01$, $d_c \approx 0.1\mu$, $v \approx 0.005\mu^3$, following Beygelzimer et al. (1994); Rybin (1986); Cheremskoj et al. (1990), respectively. Substituting these values into Eq. (40), we get $C_1 \approx 0.04$.

Assuming that the length of a free run of BNs corresponds to strain ~0.1, relationship (25) gives $C_5 \approx 10$.

According to Beygelzimer et al. (1994), $a \approx 0.1$. Then taking $p \approx 2K$, we get $C_6 \approx 1$ from relationship (40). The value of C_2 is taken to be 0.1 (see above).

Fig. 3 illustrates the solutions of system (30) for these values of parameters. We considered two loading modes: (i) quasi-monotonous loading to the equivalent strain of 0.50, and (ii) monotonous loading with two stages corresponding to strain intervals (0; 0.22) and (0.22; 0.50). In the second mode, we assume that in the beginning of the second stage, the number of AZs becomes zero.

The model shows that the intensity of grain refinement and metal damaging are smaller under a non-monotonous loading compared to a monotonous loading. This conforms experimental results (Kolmogorov, 1997).

Fig. 4 plots the space of solutions of system (30) for a quasi-monotonous loading to large values of equivalent strain. We consider two types of loading differing in the value of parameter α. The figure

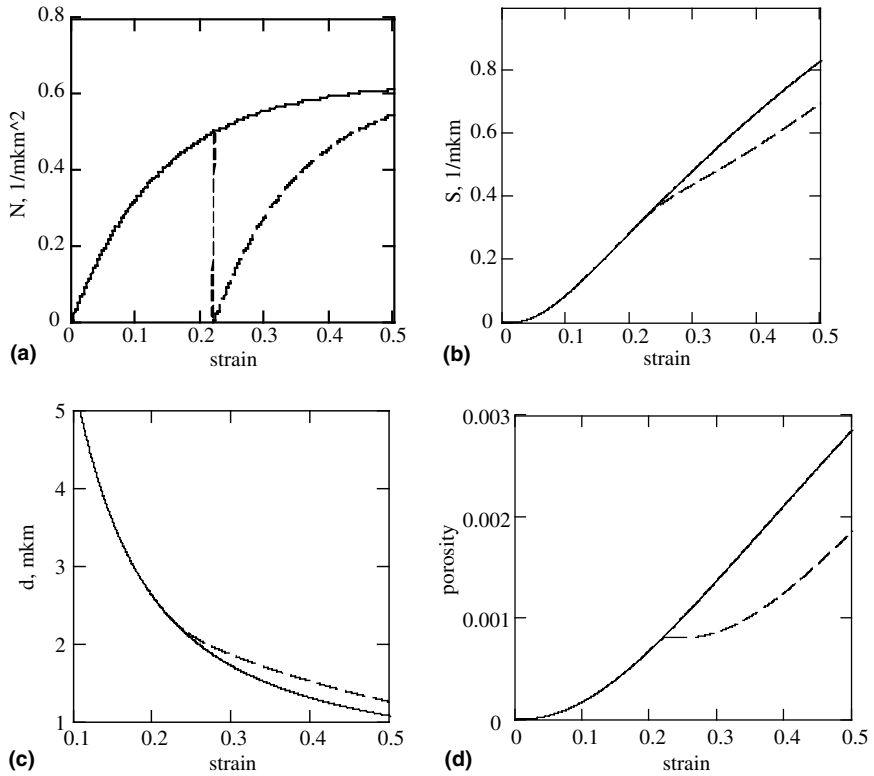

Fig. 3. Characteristics of material structure as a function of strain for monotonous (solid line) and non-monotonous (dotted line) loading: (a) number of AZs per unit cross-section area; (b) length of large-angle boundaries per unit cross-section area; (c) average fragment size; (d) porosity.

shows that the loading with a higher value of α, is more effective in terms of fragmentation, but on the other hand, it leads to higher damaging (dotted line in Fig. 4d). Carrying out the second type of loading at higher hydrostatic pressure allows one to decrease damaging, which corresponds to increasing ductility (see Fig. 4d, dash-dot line); at the same time, it preserves good grain refinement qualities.

6. Hardening, failure and localization of deformation

The analysis in the previous section shows that there are four qualitatively different stages of the quasi-monotonous loading process, provided that $C_2 \ll 1 + \frac{C_3}{C_4}$:

(i) A non-stationary stage, during which the number of AZs per unit volume grows rapidly with strain. This stage is realized when $0 < \gamma < \gamma^*$.
(ii) A quasi-stationary stage characterized by a stabilization of the number of AZs per unit volume. This stage is realized when $\gamma < \gamma^*$ and $\overline{S}_0 \ll \overline{S} \ll 1$. Grain division is self-similar during this stage.
(iii) Intense decrease of the number of AZs per unit volume. This stage is realized as $\overline{S}$ tends to 1.
(iv) Ideal plasticity when $\overline{S} = 1$ and $\overline{N} = 0$.

During the first stage, a metal is being hardened mainly because of the increase in internal stresses. During the second stage, the internal stresses are stabilized, and hardening is essentially due to an

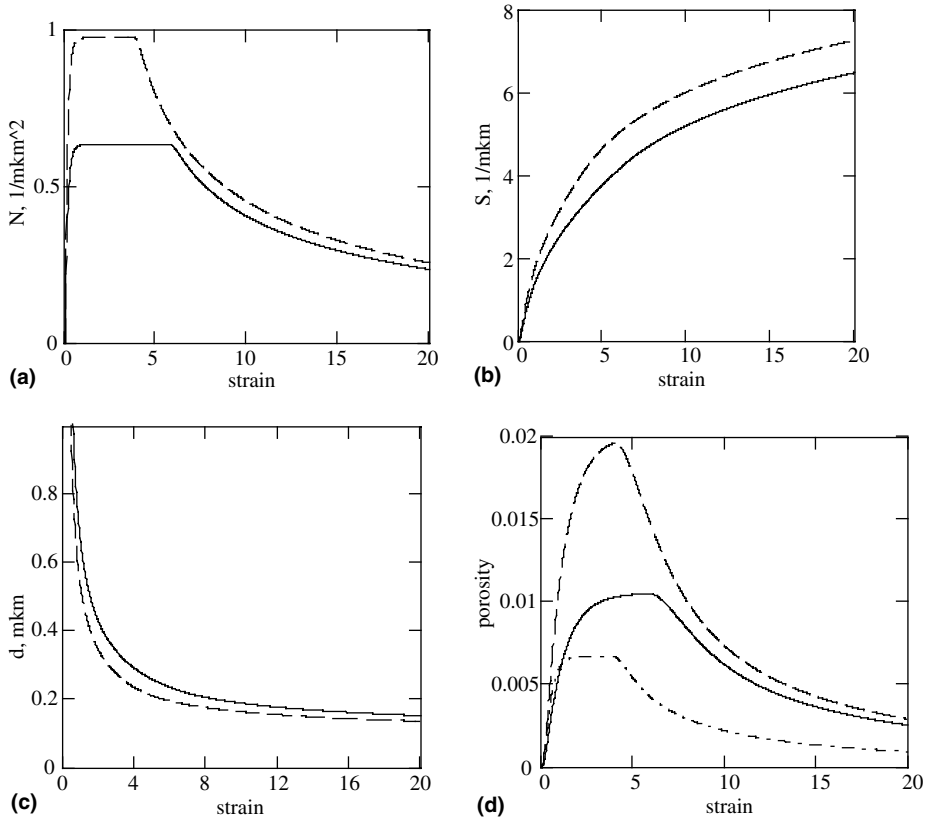

Fig. 4. Characteristics of material structure as a function of strain for quasi-monotonous loading for two types of stress state corresponding to two different values of parameter α. Solid curves corresponds to $\alpha = 0.01$, $p = 2K$; dotted to $\alpha = 0.02$, $p = 2K$; dashed-dotted to $\alpha = 0.02$, $p = 6K$. (a) number of AZs per unit of cross-section area; (b) length of high angular boundaries per unit of cross-section area; (c) average fragment size; (d) porosity.

increase in the area of high angular boundaries per unit volume of material.

If we assume that, during this stage, the work of external forces is spent mainly on sliding along disorientation boundaries, then it follows from the balance of work done by internal and external forces that

$$\sigma_s \sim \overline{S}. \tag{45}$$

Taking into account (44), we have

$$\sigma_s \sim \sqrt{\gamma}. \tag{46}$$

Notice that this dependence is often observed experimentally (Bell, 1973).

During the final stage of deformation, there is no hardening and σ_s is defined by the value of S_c.

We show that a dependence of the Hall–Petch type follows from the self-similarity of the grain refinement process (Hall, 1951; Petch, 1953).

Imagine a unit area in a cross-section of the representative volume element, and fix the mesh of high angular boundaries during consecutive steps of loading. We will take a unit length interval on each mesh and calculate the number M of points of its intersection with the boundaries. From the self-similarity of the ensemble of boundaries, it follows that the total length S of boundaries is related to M via the scaling law (de Gennes, 1979):

$$\overline{S} \sim \overline{\mathbf{M}}^{\eta}, \tag{47}$$

where η is a parameter.

A quantity reciprocal to $\overline{\mathbf{M}}$ is equal to the average size of fragments $\overline{d}$ (Chernyavsky, 1977).

It follows from the latter relationship that, in the case of scaling,

$$\overline{S} \sim \frac{1}{\overline{d}^{\eta}}. \tag{48}$$

Let us clarify the sense of parameter η. Because of self-similarity, consecutive meshes of high angular boundaries represent pre-fractals of a fractal set, where $\overline{d}$ defines the scale of each pre-fractal. From the theory of fractal sets (Mandelbrot, 1983), the length of a pre-fractal is related to its scale through the following relationship:

$$\overline{S} \sim \frac{1}{\overline{d}^{D-1}}, \tag{49}$$

where D is the fractal dimensionality of the set.

For fractal lines, $1 < D < 2$. We have $\eta = D-1$ and $0 < \eta < 1$. During the second stage of deformation η is constant.

At the start of the third stage, the self-similarity disappears and the value of η changes. Since the intensity of grain division swiftly decreases when $\overline{d} \to 1$, fragment sizes tend to equalize. It is not hard to see that in this case

$$\overline{S} \sim \frac{1}{\overline{d}}, \tag{50}$$

i.e., $\eta \to 1$.

According to relationship (45), it follows from (48) and (50) that during the second stage of loading

$$\sigma_s \sim \frac{1}{\overline{d}^{\eta}}, \tag{51}$$

and during the third stage

$$\sigma_s \sim \frac{1}{\overline{d}}. \tag{52}$$

Dependences (50) and (52) conform with experimental results (Thompson, 1977; Kim et al., 2000).

As mentioned above, the self-similarity implies differential Eq. (37) for micro-porosity. This equation corresponds to kinetic Eq. (38) from the paper (Beygelzimer et al., 1994). The later paper develops a theory of failure and deformation localization in metals under quasi-monotonous loading. The current model allows one to study these process under non-monotonous loading.

To make it possible, we need to supplement the system of Eq. (30) by appropriate constraints (Beygelzimer et al., 1994):

(i) fracture constraint:

$$\Theta = \Theta_c, \tag{53}$$

(ii) deformation localization constraint:

$$\frac{d\tau}{d\gamma} \leqslant 0, \tag{54}$$

where

$$\tau = \sqrt{\varphi(\Theta)}\sqrt{(1-\Theta)(k_0 + \alpha^* p)^2 - \frac{p^2}{\psi(\Theta)}} \tag{55}$$

is the intensity of stress deviator in a representative volume element of a porous material under plastic deformation:

$$\psi(\Theta) = \frac{(1-\Theta)^{2n-1}}{6a\Theta^m}, \quad \varphi(\Theta) = (1-\Theta)^{2n-1},$$

n and m are parameters of the material; and k_0 is the shear yield stress of the material under plastic deformation ($k_0 = \frac{\sigma_s}{\sqrt{3}}$).

Parameter α in relationship (55), taken from (Beygelzimer et al., 1994), is marked with an asterisk, since it should be substituted by the corresponding generalized quantity. Comparing the last equation of system (30) with (38) gives

$$\alpha^* = C_3 \overline{N}^{\frac{3}{2}} d_c^{-3} v. \tag{56}$$

In contrast to parameter α of the model of (Beygelzimer et al., 1994), this quantity is no longer a constant. Both parameters, however, reflect the ability of structural elements to accommodate to each other during the plastic deformation. Thus we will still call α^* the "accommodation parameter". According to (Beygelzimer et al., 1994), this parameter characterizes the ductility of the material (under the same level of pressure); the smaller this parameter, the higher the ductility.

Fig. 5 shows the values of the accommodation parameter as a function of deformation intensity

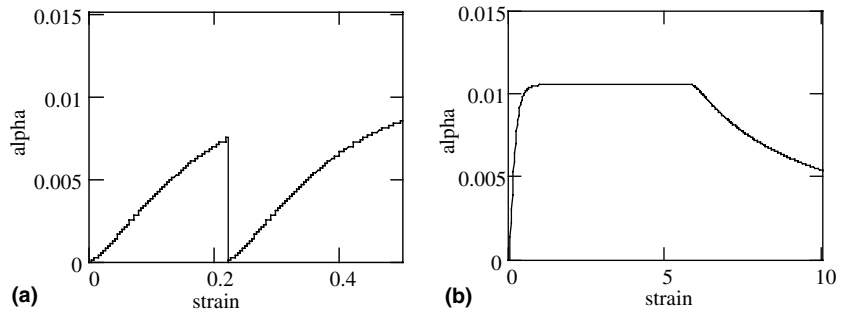

Fig. 5. Accommodation parameter as a function of equivalent strain for non-monotonous (a) and quasi-monotonous (b) loading.

under (a) quasi-monotonous and (b) non-monotonous loading. We note two interesting phenomena illustrated by the figure. First, ductility is higher for non-monotonous loading, as shown in Fig. 5 (a). This was observed before experimentally (see Kolmogorov, 1997). This effect is captured by our model since as the loading direction changes, the number of sites where nucleation of micropores can take place decreases. In this case, deformation under pressure results in healing of micropores present in the material (see Fig. 3d and the last equation in system (30)).

The second phenomenon is the increase in plasticity as a result of large plastic deformations under pressure (Fig. 5b). In our model, this phenomenon is related to the relaxation of internal stress due to slippage of small fragments along high angular boundaries of deformation origin.

7. Conclusion

The model proposed here allows to draw the following conclusions:

1. In the process of grain division, there is a limiting grain size, which can be reached under sufficiently strain and pressure. This limiting size depends on temperature, pressure, strain rate, but is independent of the stress–strain mode.
2. To increase the intensity of grain refinement and to decrease failure, it is necessary to increase the hydrostatic pressure in the center of deformation.
3. Nonmonotonous (and in particular cyclic) loading gives less intensive grain refinement and less intensive failure than quasi-monotonous loading.
4. An ultra-fine grained (UFG) structure of a given metal is obtained faster by those processes that lead to a larger decrease in ductility of this metal (under the same level of hydrostatic pressure in the center of deformation). In order to obtain a UFG structure, it is necessary to carry out these processes under high hydrostatic pressure in the center of deformation. In this case, the relaxation of internal stress happens along the direction of crystalline fragmentation, not the direction of micropores formation.
5. A microstructure with limiting grain size guarantees each metal its ideal plasticity under pressure, in the sense that the deformation is fracture- and hardening-free.

References

Barenblatt, G., 1979. Similarity, Selfsimilarity and Intermediate Asymptotics. New York, Plenum, p. 206.

Bell, D.F., 1973. Experimental foundation of solids mechanic. In: Flugge, S. (Ed.), The Encyclopedia of Physics, vol. VIa/1. In: Trusdell, C. (Ed.), Mechanics of Solids 1. Springer-Verlag, Berlin, p. 430.

Beygelzimer, Y.Y., Orlov, D.V., Varyukhin, V.N. 2002. A new severe plastic deformation method: twist extrusion. In: Zhu, Y.T., Langdon, T.G., Mishra, R.S., Semiatin, S.L., Saran, M.J., Lowe, T.C. (Eds.), Ultrafine Grained Materials II. Proceedings of a Symposium, Held During the 2002 TMS

Annual Meeting I Seattle, Washington, February 17–21, 2002. pp. 297–304.

Beygelzimer, Y.Y., Spuskanyuk, A.V., 1999. The thick yield surface: idea and approach for investigating its structure. Philos. Mag. A 79 (10), 2437.

Beygelzimer, Y.Y., Spuskanyuk, A.V., Varyukhin, V.N., 2001. On The Loading Surface of Microinhomogeneous Materials/Resent Development in Computer Modeling of Powder Metallurgy Processes. IOS Press, London, pp. 17–28.

Beygelzimer, Y.Y., Efros, B.M., Varyukhin, V.N., Khokhlov, A.V., 1994. Continuum model of the structural—inhomogeneous porous body and its application for the study of stability and viscous fracture of materials deformed under pressure. Engng. Fract. Mech. 48 (5), 629.

Cheremskoj, P.G., Slezov, V.V., Betekhtin, V.I., 1990. Pores in a Solid. Energoatomizdat, Moscow, p. 376 (in Russian).

Chernyavsky, K.S., 1977. Stereology and Material Science. Metallurgia, Moscow, p. 279 (in Russian).

de Gennes, P.-G., 1979. Scaling Concepts in Polymer Physics. Cornell University Press, Ithaca and London, p. 367.

Frost, H.J., Ashby, M.F., 1982. Deformation Mechanism Maps. Pergamon Press, Oxford, p. 322.

Hall, E.O., 1951. Proc. Roy. Soc. (London) B 64, 474.

Kim, H.S., Estrin, Y., Bush, M.B., 2000. Plastic Deformation Behavior of Fine-Grained Materials. Acta Mater. 48, 493.

Kolmogorov, A.N., 1941. On lognormal law of particle size distribution during crushing. Dokl. Acad. Nauk SSSR 31, 99 (in Russian).

Kolmogorov, V.L., 1997. Model of metal fracture in cold deformation and plasticity resource restoration in annealing. In: Predeleanu, M., Gilormini, P. (Eds.), Advanced Methods in Materials Processing Defects. Elsevier, Amsterdam, p. 417.

Langford, G.A., 1970. Study of the Deformation of Patented Steel Wire. Metall. Trans. 1, 465.

Langford, G., Cohen, M., 1975. Microstructural analysis by high-voltage electron diffraction of severely drawn. Metall. Trans. A 6, 901.

Langford, G., Cohen, M., 1969. Starin hardening of iron by severe plastic deformation. Trans. ASM 62, 623.

Mandelbrot, B., 1983. The Fractal Geometry of Nature. W.H.Freeman and Company, New York, 468.

Nemat-Nasser, S., Hori, M., 1999. Micromechanics: Overall Properties of Heterogeneous Materials. Elsevier, Amsterdam, p. 786.

Petch, N.J., 1953. J. Iron Steel Inst. 174, 25.

Raabe, D., 1998. Computational Material Science. The Simulation of Materials Microstructures and Properties. Wiley, VCH, New York, p. 379.

Rybin, V.V., 1986. High plastic deformation and fracture of metals. Metallurgia, Moscow, p. 224 (in Russian).

Segal, V., 2002. Severe plastic deformation: simple shear versus pure shear. Mater. Sci. Engng. A 338, 331.

Thompson, A., 1977. Substructure Strengthening Mechanisms. Metall. Trans. A 8, 833.

Tvergaard, V., 1992. Applications of plastic material model. In: Andersen, S.I., et al. (Eds.), Proceedings of 13th Riso International Symposium on Materials Science: Modeling of Plastic Deformation and its Engineering Applications. Riso National Laboratory, Roskilde, Denmark.

Valiev, R.Z., Islamgaliev, I.V., Alexandrov, I.V., 2000. Bulk nanostructured materials processed by severe plastic deformation. Progr. Mater. Sci. 45, 103.